*Bulgarian Chemical Communications, Volume 58, Special Issue A (pp. 49-53) 2026 DOI: 10.34049/bcc.58.A.SN-09*

# Synthesis and physicochemical characterization of rhodium(III) hydrogenselenite

K. Todorova, V. Georgieva*, S. Genieva

*Department of Chemistry, Burgas State University "Prof. Dr. Assen Zlatarov'', 1 Prof. Yakimov Str., 8010 Burgas, Bulgaria*

Received: July 9, 2025; Accepted: November 09, 2025

The present study examines the hydrothermal approach for the synthesis of rhodium(III) hydrogenselenite, determining its structural features and potential functional properties. The precursors of the synthesis are rhodium trichloride trihydrate ($RhCl_3 \cdot 3H_2O$) and sodium hydrogenselenite ($NaHSeO_3$), in stoichiometric quantities, duration 100 hours and temperature 200°C. For good crystallinity of the product, additional hydrothermal treatment was performed in an optimal pH environment. Orange-brown crystalline phase with a probable chemical composition of rhodium hydrogenselenite ($Rh(HSeO_3)_3$) was obtained. Various physicochemical methods of analysis, including Fourier transform infrared spectroscopy (FTIR), X-ray diffraction (XRD), and ultraviolet-visible spectroscopy (UV-vis), were employed to elucidate the composition of the solid phases obtained.

**Keywords:** hydrothermal synthesis, rhodium oxoselenates, physicochemical analysis

## INTRODUCTION

Platinum-group metals are distinguished by their exceptional catalytic properties, making them indispensable in various industrial and environmental applications [1–3]. These properties stem from their unique electronic configurations, particularly the partially filled d-orbitals, which enable the formation of diverse coordination environments and reaction pathways. The catalytic performance of these metals can be finely tuned by incorporating ligands with specific optical, magnetic, or biological functionalities, allowing precise control over reactivity, selectivity, and stability [4].

Among these, rhodium is particularly noteworthy for its versatility across multiple oxidation states (+I to +V), and its broad functional-group tolerance and high stability in aqueous environments [5–7]. Rhodium complexes, in particular, are widely employed in homogeneous catalysis for hydrogenation, hydroformylation, and hydrosilylation reactions [8–10]. These reactions are essential for the synthesis of fine chemicals and intermediates in the pharmaceutical and petrochemical industries [11, 12]. Beyond catalysis, rhodium-based compounds have garnered attention in medicinal and diagnostic research due to their ability to engage with specific biomolecular targets [13–15].

Recent studies have identified oxygen-containing selenium ions, such as selenite ($SeO_3^{2-}$) and selenate ($SeO_4^{2-}$), as effective and stable ligands that can enhance the structural adaptability and reactivity of metal complexes [16]. The combination of selenium-based ligands with rhodium creates opportunities to design novel coordination compounds with multifunctional properties relevant to catalysis, materials science, and therapeutics.

Rhodium oxoselenates, in particular, represent a relatively underexplored class of compounds that merge the complex coordination chemistry of rhodium with the diverse structural frameworks of selenium oxyanions. Their potential utility spans through heterogeneous catalysis, electrochemical systems, and functional materials with tunable electronic and magnetic properties. In higher oxidation states (+III to +V), rhodium forms structurally robust but synthetically challenging compounds that remain the subject of ongoing crystallographic and spectroscopic investigations [17–19].

Accordingly, the aim of the present study was to synthesize rhodium(III) hydrogenselenite and to perform comprehensive physicochemical characterization to evaluate its potential for future applications.

## EXPERIMENTAL

Hydrothermal synthesis was conducted using rhodium trichloride ($RhCl_3$) and sodium hydrogenselenite ($NaHSeO_3$) in the following quantities: 1.06 g (5.05 mmol) $RhCl_3 \cdot 3H_2O$, 2.17 g (14.37 mmol) $NaHSeO_3$, and 20 ml (1111.11 mmol) $H_2O$. The synthesis was carried out at 200°C for 100 h in 50 ml stainless steel autoclaves with an internal Teflon coating. An orange-colored maternal solution containing a precipitate of deep orange color was

* To whom all correspondence should be sent:
E-mail: *velyana_topalska@btu.bg*

obtained. This precipitate was subsequently separated from the solution by decanting. After drying at 60°C, an orange-brown solid phase of $Rh(HSeO_3)_3$ was formed for a day (Fig. 1).

a

**Fig. 1.** Photograph of the product obtained in the system $RhCl_3 \times 3H_2O/NaHSeO_3$

Surface functional groups in the synthesized sample and output reagents were characterized using a Nicolet iS50 FT-IR spectrometer which detects characteristic absorption bands in the mid-infrared region (400–4000 $cm^{-1}$), corresponding to various valence and deformation vibrations of chemical bonds. Electronic transitions in the molecules were monitored using UV-vis spectroscopy. Spectra were recorded at room temperature with an Evolution 300 spectrophotometer operating in the wavelength range of 190 – 1000 nm. Spectralon was used as the reference standard. The phase composition of the samples was determined using a Bruker D8 Advance X-ray diffractometer with Cu $K_\alpha$ radiation (λ = 0.15406 nm) and a PW 2200 Bragg-Brentano θ/2θ goniometer. Diffraction patterns were collected over a 2θ range of 10–90°, with a step size of 0.033° and a counting time of 10.0 s per step. Phase identification was carried out using standard database patterns.

## RESULTS AND DISCUSSION

The Fourier transform infrared spectra (FTIR) of the synthesized sample and of the output reactants in the reaction systems are presented in Fig. 2.

In the high-frequency region of the spectra (3600–3200 $cm^{-1}$), distinctive absorption bands are observed, corresponding to the stretching vibrations of O–H bonds in the studied compounds or in associated crystallization water. In the medium-frequency region of FTIR spectra (1630–1610 $cm^{-1}$), absorption peaks corresponding to deformation vibrations of O–H bonds were recorded. In the low-frequency region (1000–400 $cm^{-1}$), identified peaks were associated with the stretching vibrations of Se–O bonds in the $SeO_3^{2-}$ ion and in the $SeO_2$ molecule [20–23].

In the FTIR spectrum of $NaHSeO_3$ (Fig. 2, spectrum 1), characteristic absorption bands are observed at 3451 $cm^{-1}$ and 2429 $cm^{-1}$, corresponding to the symmetric stretching vibrations ($\nu_s$) of H–O bonds. Bending vibrations (δ) of H–O bonds were detected at 1636 $cm^{-1}$ and 1234 $cm^{-1}$. Bands at 890 $cm^{-1}$, 845 $cm^{-1}$ and 823 $cm^{-1}$ were attributed to symmetric stretching vibrations ($\nu_s$) of the $SeO_2$ unit, while the band at 788 $cm^{-1}$ corresponds to the asymmetric stretching vibration ($\nu_{as}$) of Se–O. Additional bands at 614 $cm^{-1}$, 599 $cm^{-1}$ and 429 $cm^{-1}$ were assigned to O–Se–O bending (valence) vibrations [24–26].

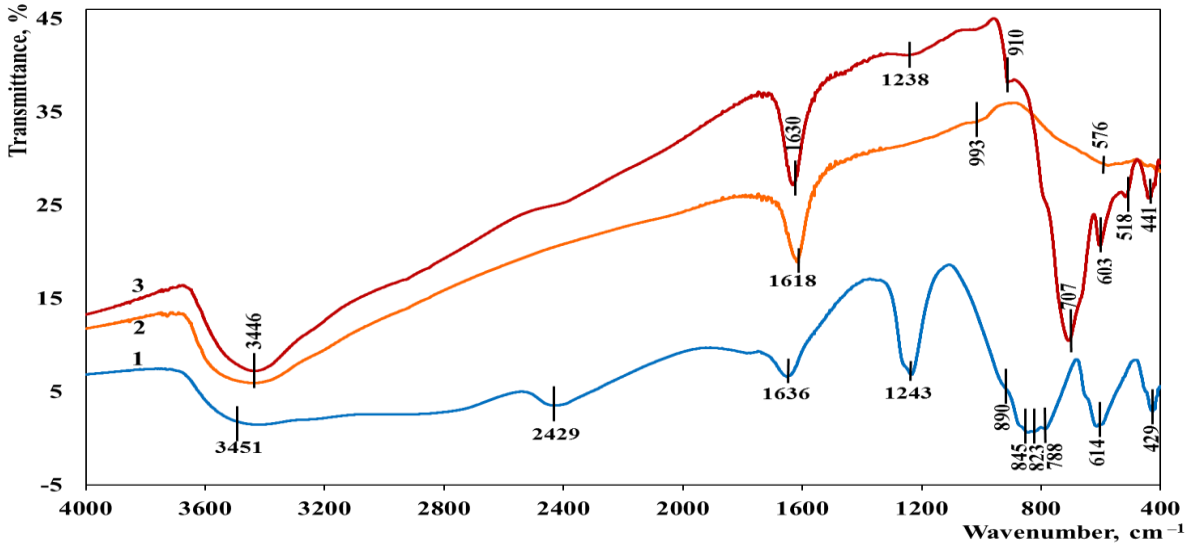


**Fig. 2.** FTIR spectra of: 1 – $NaHSeO_3$, 2 –$RhCl_3 \times 3H_2O$, 3 – $Rh(HSeO_3)_3$

$RhCl_3 \cdot 3H_2O$ (Fig. 2, spectrum 2) exhibits absorption bands at 3446 $cm^{-1}$, 1618 $cm^{-1}$, and 543 $cm^{-1}$, corresponding to the stretching and bending vibrations of O–H bonds from crystallization water. Additional bands attributed to the stretching and deformation vibrations of Rh–Cl bonds are observed below 400 $cm^{-1}$ [27].

The FTIR spectrum of the synthesized compound $Rh(HSeO_3)_3$ (Fig. 2, spectrum 3) displays absorption bands corresponding to the stretching and bending vibrations of O–H bonds, observed at 3446 $cm^{-1}$ and 1630 $cm^{-1}$, indicating the presence of crystallization water. Additional bands appear at 910 $cm^{-1}$, 707 $cm^{-1}$, 603 $cm^{-1}$, 518 $cm^{-1}$ and 441 $cm^{-1}$. Several of these are shifted relative to the characteristic bands of $NaHSeO_3$, and were attributed to symmetric $SeO_2$ stretching ($\nu_s$), asymmetric Se–O stretching ($\nu_{as}$), and O–Se–O stretching vibrations (especially at 603 $cm^{-1}$). The bands at 518 $cm^{-1}$ and 441 $cm^{-1}$ were attributed to symmetric Se–OH stretching and bending vibrations, respectively, providing evidence for the presence of the hydrogenselenite ($HSeO_3^-$) ion [26].

UV–vis spectroscopy was employed to confirm the composition of the synthesized solid phase. The UV–vis spectra of the studied reaction system are shown in Fig. 3.

The UV–vis spectrum of $NaHSeO_3$ (Fig. 3) shows a high-energy absorption band with a maximum at 228 nm, corresponding to transitions at the highest energy level. In addition, a broad absorption band centered at 499 nm is observed. This band was attributed to a sodium-induced intraligand $\pi \rightarrow \pi^*$ transition, likely influenced by the filled p-electron configuration of the $Na^+$ ion [28]. The spectrum of the parent compound $RhCl_3 \times 3H_2O$ (Fig. 3) is characterized by a less intense band at 242 nm and a broad absorption band with a maximum at 549 nm.

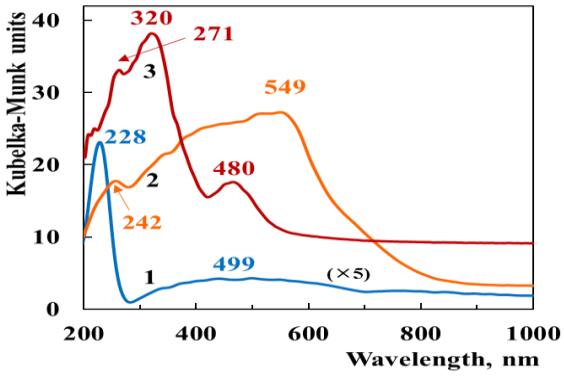


**Fig. 3.** UV-vis spectra of: 1 – $NaHSeO_3$, 2 – $RhCl_3 \times 3H_2O$, 3 – $Rh(HSeO_3)_3$

These features are consistent with ligand-to-metal charge transfer (LMCT) and d–d transitions typical of rhodium(III) complexes in octahedral coordination environments [29]. The UV–vis spectrum of the synthesized $Rh(HSeO_3)_3$ complex (Fig. 3) reveals three distinct and intense absorption bands at 271 nm, 320 nm, and 480 nm. The band at 320 nm corresponds to the highest energy transition in this compound. These absorption features are consistent with electronic transitions reported in other selenium- and rhodium-containing compounds [30], and are also comparable to transitions observed in certain organometallic rhodium complexes [31, 32]. The presence of strong absorption in both the UV and visible regions suggests that $Rh(HSeO_3)_3$ may have promising applications in photocatalysis and light-driven redox processes. Its electronic absorption profile, particularly the band at 480 nm in the visible range, indicates potential utility as a visible-light-responsive material. Such characteristics are desirable for the development of catalytic systems, light-activated sensors, or functional materials in optoelectronic devices [33, 34]. The compound's responsiveness to both UV and visible light also points to possible roles in environmental remediation technologies, such as photodegradation of organic pollutants or solar-driven water splitting.

In the X-ray diffraction (XRD) pattern of $NaHSeO_3$ (Fig. 4), intense diffraction peaks were recorded at $2\theta$ values of 17.7°, 25.7°, 26.8°, 27.6°, 29.4°, 30.4°, 30.9°, 32.4°, 33.8°, 34.9°, 35.8°, 41.3°, 46.3°, and 54.4°, in agreement with the reference pattern ICSD 00-032-1088.

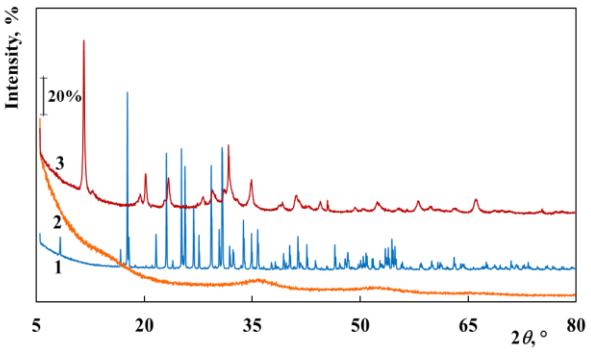


**Fig. 4.** X-ray diffraction pattern of: 1 – $NaHSeO_3$, 2 – $RhCl_3 \times 3H_2O$, 3 – $Rh(HSeO_3)_3$

The reference compound $RhCl_3 \times 3H_2O$ displayed an amorphous profile, with no distinct diffraction peaks detected (Fig. 2, 2). According to Zhou *et al.* [35], its main characteristic peaks are located at 9.49°, 36.75°, 52.75°, and 65.94°, further supporting the amorphous nature of the sample analyzed here. In contrast, the XRD pattern of the synthesized

$Rh(HSeO_3)_3$ compound (Fig. 4) exhibits well-defined reflections at $2\theta$ values of 11.6°, 20.1°, 23.5°, 31.6°, and 34.9°. However, no corresponding phase was found in the ICSD database, suggesting the formation of a previously unreported crystalline phase. Ongoing efforts are focused on identifying an isostructural analogue to support the qualitative characterization of this new compound. Preliminary crystallographic analysis indicates that the compound crystallizes in the orthorhombic Pmmm space group, with unit cell parameters a = 15.149(3) Å, b = 13.694(2) Å, and c = 4.4028(1) Å. Further crystallization attempts, conducted at 200 °C in 0.2 M NaOH solution over a two-week period, did not alter the diffraction pattern, and no single crystals suitable for structure determination were obtained.

## CONCLUSIONS

In this study, a new rhodium hydrogenselenite compound, $Rh(HSeO_3)_3$, was synthesized for the first time through a reaction between $RhCl_3{\times}3H_2O$ and $NaHSeO_3$ under mild hydrothermal conditions. The structure and composition of the product were investigated using FTIR, UV–vis spectroscopy, and X-ray powder diffraction (XRD).

FTIR spectroscopy confirmed the presence of hydrogenselenite ligands and crystallization water in the structure, as indicated by characteristic O–H and Se–OH vibrational bands. The UV–vis spectral profile of the compound revealed three distinct absorption bands at 271, 320, and 480 nm, corresponding to electronic transitions associated with both selenium and rhodium centers. The absorption in the visible region suggests that $Rh(HSeO_3)_3$ may be a suitable candidate for applications in photocatalysis, solar energy conversion, and photoresponsive materials.

XRD analysis of the synthesized material demonstrated a crystalline phase with clearly defined diffraction peaks not matching any known compound in the ICSD database, confirming the formation of a new phase. Preliminary crystallographic analysis suggests an orthorhombic crystal system with Pmmm symmetry and unit cell parameters a = 15.149(3) Å, b = 13.694(2) Å, and c = 4.4028(1) Å. Although prolonged crystallization under alkaline conditions at 200 °C did not yield single crystals suitable for full structural determination, the reproducibility of the diffraction pattern confirms the phase stability.

The successful synthesis and initial characterization of $Rh(HSeO_3)_3$ provide a basis for further structural and functional investigation. The compound's light absorption properties and the redox-active nature of both rhodium and selenium open avenues for its use in environmental remediation, catalytic hydrogenation, and sensor development. Future work will focus on optimizing crystallization conditions to enable single-crystal X-ray diffraction studies and exploring the compound's catalytic behavior under photochemical and electrochemical conditions.

## REFERENCES


1. K. Nose, T. H. Okabe, in: Treatise Process Metall., Elsevier, UK, 2014, p. 1071.
2. A. E. Hughes, N. Haque, S. A. Northey, S. Giddey, *Resources*, **10**, 1 (2021).
3. H. Tang, Z. Peng, R. Tian, L. Ye, J. Zhang, M. Rao, G. Li, *J. Environ. Chem. Eng.*, **11**, 110237 (2023).
4. S. Swaminathan, P. Jerome, R. J. Deepak, R. Karvembu, T. H. Oh, *Coord. Chem. Rev.*, **503**, 215620 (2024).
5. Z. Wu, K. L. Hull, *Chem. Sci.*, **7**, 969 (2016).
6. J. Hansen, H. M. L. Davies, *Coord. Chem. Rev.*, **252**, 545 (2008).
7. S. Kim, S. Han, J. Park, S. Sharma, N. K. Mishra, H. Oh, J. H. Kwak, I. S. Kim, *Chem. Commun.*, **53**, 3006 (2017).
8. W. Gil, A. M. Trzeciak, *Coord. Chem. Rev.*, **255**, 473 (2011).
9. J. P. Morales-Cerón, P. Lara, J. López-Serrano, L. L. Santos, V. Salazar, E. Álvarez, A. Suárez, *Organometallics*, **36**, 2460 (2017).
10. S. Medici, M. Peana, A. Pelucelli, M. A. Zoroddu, *Molecules*, **26**, 2553 (2021).
11. Y. Wei, B. Rao, X. Cong, X. Zeng, *J. Am. Chem. Soc.*, **137**, 9250 (2015).
12. P. Govender, S. Ngubane, B. Therrien, G. S. Smith, *J. Organomet. Chem.*, **848**, 281 (2017).
13. J. Bianga, N. Kopplin, J. Hülsmann, D. Vogt, T. Seidensticker, *Adv. Synth. Catal.*, **362**, 4415 (2020).
14. M. C. Simpson, D. J. Cole-Hamilton, *Coord. Chem. Rev.*, **155**, 163 (1996).
15. P. Peng, B. U. Xianhui, N. Zheng, *Acc. Chem. Res.*, 38, 293 (2005).
16. M. S. Wickleder, C. Logemann, in: Handbook of Chalcogen Chemistry: New Perspectives in Sulfur, Selenium and Tellurium, F. Devillanova, W.-W. Du Mont (eds.), Royal Society of Chemistry, Cambridge, UK, 2013, p. 307.
17. D. L. Ma, M. Wang, Z. Mao, C. Yang, C. T. Ng, C. H. Leung, *Dalt. Trans.*, **45**, 2762 (2016).
18. M. Sohrabi, M. Saeedi, B. Larijani, M. Mahdavi, *Eur. J. Med. Chem.*, **216**, 113308 (2021).
19. S. J. Thompson, M. R. Brennan, S. Y. Lee, G. Dong, *Chem. Soc. Rev.*, **47**, 929 (2018).
20. V. P. Verma, *Thermochim. Acta*, **327**, 63 (1999).
21. D. M. Calderón, U. Morales, C. Velásquez, V. H. Lara, L. Salgado, *Catal. Letters*, **132**, 268 (2009).
22. A. D. Allen, T. Theophanides, *Can. J. Chem.*, **42**, 1 (1964).
23. O. Janson, W. Schnelle, M. Schmidt, Y. Prots, S. L. Drechsler, S. K. Filatov, H. Rosner, *New J. Phys.*, **11**, (2009).

24. J. Stangret, T. Gampe, *J. Phys. Chem. A*, **106**, 5393 (2002).
25. L. Eklund, I. Persson, *Dalt. Trans.*, **43**, 6315 (2014).
26. J. Kretzschmar, N. Jordan, E. Brendler, S. Tsushima, C. Franzen, H. Foerstendorf, M. Stockmann, K. Heim, V. Brendler, *Dalt. Trans.*, **44**, 10508 (2015).
27. K. V. Yusenko, A. S. Sukhikh, W. Kraus, S. A. Gromilov, *Mol. 2020,* **25***,* 768 (2020).
28. S. Sutradhar, S. Basak, D. Das, B. Nath Ghosh, *Polyhedron*, **236**, 116344 (2023).
29. D. B. Vasilchenko, S. N. Berdyugin, S. V. Korenev, S. O'Kennedy, W. J. Gerber, *Inorg. Chem.*, **56**, 10724 (2017).
30. A. P. Ginsberg, W. E. Lindsell, C. R. Sprinkle, K. W. West, R. L. Cohen, *Inorg. Chem.*, **21**, 3666 (1982).
31. W. L. Su, Y. Cheng Yu, M. Ching Tseng, S. P. Wang, W. L. Huang, *J. Chem. Soc. Dalt. Trans.*, 3440 (2006).
32. T. Vadivel, M. Dhamodaran, S. Kulathooran, S. Kavitha, K. Amirthaganesan, S. Chandrasekaran, N. Ilayaraja, S. Senguttuvan, *Carbohydr. Res.*, **487**, 107878 (2020).
33. X. Cheng, D. Li, B. Yang, Y. Lin, L. Gong, *Chinese J. Org. Chem.*, **42**, 3335 (2022).
34. F. Camara, T. Gavaggio, B. Dautreppe, J. Chauvin, J. Pécaut, D. Aldakov, M.-N. Collomb, J. Fortage, *Molecules*, **27**, 6614 (2022).
35. W. Zhou, J. Yi, J. Lin, S. Fang, X. Peng, *Res. Chem. Intermed.*, **43**, 3651 (2017).
36. R. E. Morris, W. T. A. Harrison, G. D. Stucky, A. K. Cheetham, *J. Solid State Chem.*, **94**, 227 (1991).